
Article:
Vanon, R. and Ohkitani, K. (2018) Applications of a Cole-Hopf transform to the 3D Navier-Stokes equations. Journal of Turbulence, 19 (4). pp. 322-333. ISSN 1468-5248

https://doi.org/10.1080/14685248.2018.1431395

ARTICLE TEMPLATE

Applications of a Cole-Hopf transform to the 3D Navier-Stokes equations

Riccardo Vanon and Koji Ohkitani

School of Mathematics and Statistics, University of Sheffield, Hicks Building, Hounsfield Road, Sheffield S3 7RH, UK

ARTICLE HISTORY
Compiled December 18, 2017

ABSTRACT
The Navier-Stokes equations written in the vector potential can be recast as the nonlinear Schrödinger equations at imaginary times, i.e. the heat equations with a potential term, using the Cole-Hopf transform introduced in Ohkitani(2017). On this basis, we study two kinds of Navier-Stokes flows by means of direct numerical simulations. In an experiment on vortex reconnection, it is found that the potential term takes large negative values in regions where intensive reconnection is taking place, whereas the signature of the nonlinear term is more broadly spread. For decaying turbulence starting from a random initial condition, such a correspondence is also observed in the early stage when the flow is dominated by vorticity layers. At later times, when the flow features several tubular vortices, this correspondence becomes weaker. Finally, a similar set of transformations is presented for the magnetohydrodynamic equations, which reduces them to a set of heat equations with suitable potential terms, thereby obtaining new criteria for the regularity of their solutions.

KEYWORDS
Navier-Stokes equations; Cole-Hopf transform; Feynman-Kac formula; Duhamel principle

1. Introduction

Previously in [1], the Cole-Hopf transform originally developed for the Burgers equations was extended to the Navier-Stokes equations. This reduces the Navier-Stokes equations to the nonlinear Schrödinger equations at imaginary times, i.e. to the heat equations with a potential term (a forcing that depends on the unknowns). On a theoretical side, such an analogue of the transform has been found to be useful in obtaining a known criterion for the regularity of solutions in a straightforward fashion; on a more practical side, numerical simulations have been carried out to see how effectively the potential term captures near-singular structures in two-dimensional turbulence. While the mathematical formulation for such an approach has been described in any number of spatial dimensions, the numerical experiments were restricted to two dimensions therein.

In this paper, we present analyses of the direct numerical simulations of the three-dimensional Navier-Stokes equations on the basis of such a formalism. In particular,

CONTACT Koji Ohkitani: K.Ohkitani@sheffield.ac.uk

we will study how the potential term behaves in connection with vortex dynamics, also comparing its behaviour to that of the nonlinear term.

The rest of this work is organised as follows. In Section 2, the basic mathematical formulation of the three-dimensional Navier-Stokes equations is described. In Section 3, the analogue of the Cole-Hopf transform is briefly recalled. Section 4 comprises the main results, where we report our findings from direct numerical simulations. Two cases are described: one is a computation of vortex reconnection, the other is decaying isotropic turbulence from random initial conditions. Finally, we summarise the findings of our work in Section 5.

2. Three-dimensional Navier-Stokes equations

We consider the incompressible Navier-Stokes equations with standard notations in $\mathbb{R}^3$:

$$\begin{aligned} \frac{\partial \boldsymbol{u}}{\partial t} + \boldsymbol{u} \cdot \nabla \boldsymbol{u} &= -\nabla p + \nu \Delta \boldsymbol{u}, \\ \nabla \cdot \boldsymbol{u} &= 0, \\ \boldsymbol{u}(\boldsymbol{x}, 0) &= \boldsymbol{u}_0(\boldsymbol{x}), \end{aligned} \tag{1}$$

where the velocity $\boldsymbol{u} = \nabla \times \boldsymbol{\psi}$ has the vector potential $\boldsymbol{\psi}$ with the gauge condition $\nabla \cdot \boldsymbol{\psi} = 0$. The governing equation can also be written in terms of the vorticity $\boldsymbol{\omega} = \nabla \times \boldsymbol{u}$, resulting in

$$\frac{\partial \boldsymbol{\omega}}{\partial t} + \boldsymbol{u} \cdot \nabla \boldsymbol{\omega} = \boldsymbol{\omega} \cdot \nabla \boldsymbol{u} + \nu \Delta \boldsymbol{\omega}. \tag{2}$$

Yet another form can be obtained in terms of the vector potential $\boldsymbol{\psi}$, which is related to the vorticity by means of $\boldsymbol{\omega} = -\Delta \boldsymbol{\psi}$; this reads [4]

$$\frac{\partial \boldsymbol{\psi}}{\partial t} = \boldsymbol{T}[\nabla \boldsymbol{\psi}] + \nu \Delta \boldsymbol{\psi}, \tag{3}$$

where the non-linear term is given by

$$\boldsymbol{T}[\nabla \boldsymbol{\psi}] = \frac{3}{4\pi} \mathrm{P.V.} \int_{\mathbb{R}^3} \frac{\boldsymbol{r} \times (\nabla \times \boldsymbol{\psi}(\boldsymbol{y}))\, \boldsymbol{r} \cdot (\nabla \times \boldsymbol{\psi}(\boldsymbol{y}))}{|\boldsymbol{r}|^5} \, \mathrm{d}\boldsymbol{y}, \tag{4}$$

with $\boldsymbol{r} = \boldsymbol{x} - \boldsymbol{y}$ and P.V. standing for a principal-value integral. A similar formulation can be obtained for the system of magneto-hydrodynamic (hereafter, MHD) equations, its derivation being presented in **Appendix** A.

3. Cole-Hopf transform

In this section, we recall an analogue of the Cole-Hopf transform for the three-dimensional incompressible Navier-Stokes equations using a straightforward component-wise extension.

We introduce the Cole-Hopf transforms for each $\theta_j > 0$,

$$\psi_j = k \log \theta_j, \quad (j = 1, 2, 3), \tag{5}$$

where $\frac{1}{\theta_1}\frac{\partial \theta_1}{\partial x_1} + \frac{1}{\theta_2}\frac{\partial \theta_2}{\partial x_2} + \frac{1}{\theta_3}\frac{\partial \theta_3}{\partial x_3} = 0$. By (3) we obtain a system of heat equations

$$\frac{\partial \theta_j}{\partial t} = \nu \Delta \theta_j + f_j(\boldsymbol{x}, t)\theta_j, \quad \text{(no summation)} \tag{6}$$

where the potential term is given by

$$f_j(\boldsymbol{x}, t) = kT_j \left[\frac{\nabla \theta_1}{\theta_1}, \frac{\nabla \theta_2}{\theta_2}, \frac{\nabla \theta_3}{\theta_3} \right] - \nu \frac{|\nabla \theta_j|^2}{\theta_j^2}, \quad (j = 1, 2, 3). \tag{7}$$

If all the components f_j $(j = 1, 2, 3)$ are bounded – that is, if $\int_0^T \sup_{\boldsymbol{x}} |\boldsymbol{f}(\boldsymbol{x}, t)| dt < \infty$ on $[0, T]$ – the solutions θ_j of (6) are smooth on the same time interval, as a result of an application of the Feynman-Kac formula. As the potential term $\boldsymbol{f}$ controls the regularity of solutions, it is expected that it serves as a probe for near-singularities in the flow field. This anticipation has been justified numerically in two dimensions [1]. Here we will study whether and how the potential term can monitor near-singularities (or extreme events) in the three-dimensional flow.

A similar set of Cole-Hopf transforms can be applied to the MHD equations, resulting in a companion formalism; this is presented in **Appendix** B.

In the numerical experiments below, we simply choose $k = \nu$. We have checked that the numerical results remain qualitatively unaffected when we take $k = c\nu$ with $c \neq 1$.

4. Numerical experiments

In order to study how the potential term $\boldsymbol{f}(\boldsymbol{x}, t)$ behaves, we have carried out direct numerical simulations of the 3D Navier-Stokes equations under periodic boundary conditions.

4.1. Numerical formulation

We consider the Navier-Stokes equations in a periodic box of dimensions $[0, 2\pi]^3$. We use a standard Fourier pseudo-spectral method, employing a fourth order Runge-Kutta iteration, to evaluate the nonlinear terms. Aliasing errors are removed by the so-called 2/3-rule.

The number of grid points considered was $N = 128$ and 256 in each dimension, with the total number of points given by N^3; the time step is fixed and typically chosen to be $\Delta t = 2.5 \times 10^{-3}$. The value of the kinematic viscosity is $\nu = 7.5 \times 10^{-3}$. We have used computations with $N = 128$ for checking numerical accuracy, but the results presented in this work were all obtained using $N = 256$.

The numerical accuracy was confirmed by checking the behaviour of the energy

spectrum

$$E(k) = \frac{1}{2} \sum_{k \le |\boldsymbol{k}| < k+1} |\widetilde{\boldsymbol{u}}(\boldsymbol{k})|^2,$$

where $\widetilde{\boldsymbol{u}}(\boldsymbol{k})$ denotes the Fourier coefficient of the velocity. The spectrum shows an exponential decay at large wavenumbers k, implying that the flows are well-resolved throughout the time intervals under consideration (figure omitted).

We consider two kinds of initial conditions. In Case 1, we take a pair of orthogonally-offset vortex tubes used in the study of vortex reconnection [7]. In Case 2, we use a random initial condition whose energy spectrum is localised at lower wavenumbers

$$E(k) = ck^2 \exp(-k^2),$$

with their phases randomised. We choose c to normalise the kinetic energy $E(0) = \frac{1}{2}\left\langle |\boldsymbol{u}|^2 \right\rangle = 1$ initially, where the brackets denotes a spatial average.

We note that (3) can also be written as

$$\begin{aligned} \frac{\partial \psi_i}{\partial t} &= \epsilon_{lpq} R_j R_l \partial_p \psi_q (\partial_j \psi_i - \partial_i \psi_j) + \nu \Delta \psi_i, \\ &= \frac{1}{2} \epsilon_{lpq} R_j R_l (\partial_p \psi_q - \partial_q \psi_p)(\partial_j \psi_i - \partial_i \psi_j) + \nu \Delta \psi_i, \quad i = 1, 2, 3. \end{aligned} \tag{8}$$

Here R_j denotes the Riesz transform defined (in the whole space case) by

$$R_j[f](\boldsymbol{x}) = \frac{1}{\pi^2} \mathrm{P.V.} \int_{\mathbb{R}^3} \frac{x_j - y_j}{|\boldsymbol{x} - \boldsymbol{y}|^4} f(\boldsymbol{y}) \mathrm{d}\boldsymbol{y}.$$

The Fourier transform of R_j is given by $\widehat{R}_j = -ik_j/|\boldsymbol{k}|$, which is also valid under periodic boundary conditions. Noting that $\partial_j \psi_i - \partial_i \psi_j = \epsilon_{jil} u_l$, equation (8) reads:

$$\begin{aligned} \frac{\partial \psi_i}{\partial t} &= -\epsilon_{ijm} \partial_j \partial_l (-\Delta)^{-1} (u_l u_m) + \nu \Delta \psi_i, \\ &= T_i[\nabla \boldsymbol{\psi}] + \nu \Delta \psi_i, \end{aligned}$$

which is convenient for the numerical evaluation of the nonlinear term $T_i[\nabla \boldsymbol{\psi}]$. Its Fourier transform $\widehat{T_i[\nabla \boldsymbol{\psi}]}$ can be written as

$$\widehat{T_i[\nabla \boldsymbol{\psi}]} = \epsilon_{ijm} \frac{k_j k_l}{|\boldsymbol{k}|^2} \widehat{u_l u_m}, \tag{9}$$

where $\boldsymbol{k} = (k_1, k_2, k_3) \neq 0$ is the wavenumber. The right-hand side of the above expression can be evaluated by estimating the convolution products. In this work, we solve the Navier-Stokes equations in vorticity form using a standard method and evaluate the $\boldsymbol{f}$ and $\boldsymbol{T}[\nabla \boldsymbol{\psi}]$ terms concomitantly with the time-evolution.

4.2. Case 1: Reconnection of vortices

In order to understand the role played by the potential term $\boldsymbol{f}(\boldsymbol{x}, t)$, we first consider the simple initial condition of two orthogonal vortex tubes (such as the one used by [7] in the study of vortex reconnection).

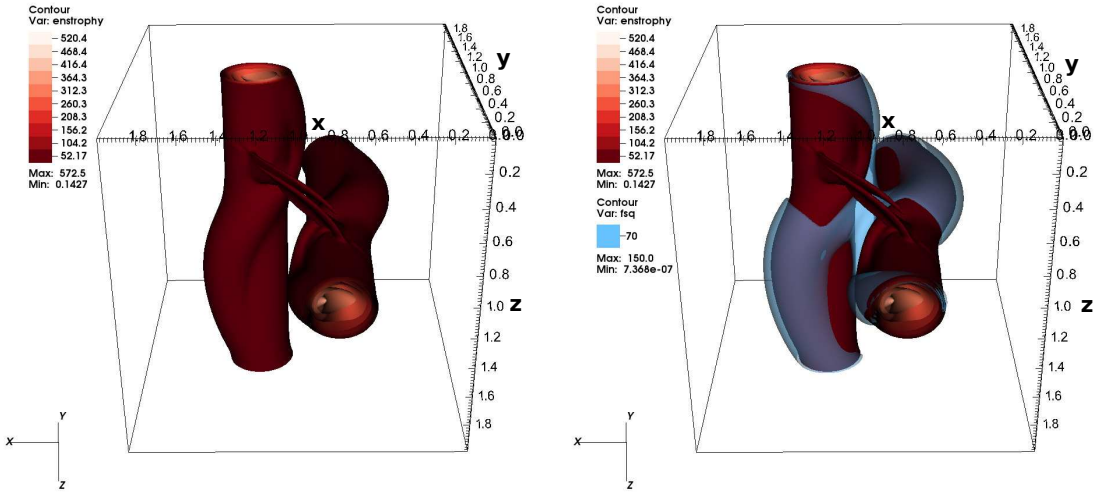

(a) (b)

Figure 1. Isosurfaces of (a) $|\boldsymbol{\omega}|^2$ (red) and (b) $|\boldsymbol{f}|^2$ (blue) overlaid on $|\boldsymbol{\omega}|^2$ (red) at $t = 1.25$.

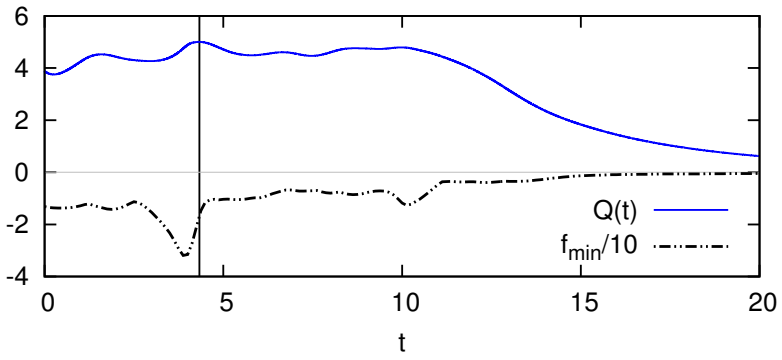

Figure 2. Time evolution of $Q(t)$ (blue, full line) and $f_{\min}$ (black, dot-dashed; scaled down by 10) for the orthogonal vortex tubes initial condition.

Figure 1 shows (a) the isosurfaces of the enstrophy and (b) those of the potential term $|\boldsymbol{f}|^2$ overlaid on the enstrophy at early times, $t = 1.25$, when the enstrophy isosurface still closely resembles the set initial conditions. Note that the characteristics of $|\boldsymbol{f}|^2$ are observed near and around the vortex tubes, as well as in the interacting zone between them.

The time evolution of the enstrophy

$$Q(t) = \frac{1}{2} \left\langle |\boldsymbol{\omega}|^2 \right\rangle$$

and that of the minimum value of $\boldsymbol{f}$

$$f_{\min}(t) = \min_{\boldsymbol{x},j} f_j(\boldsymbol{x}, t)$$

are shown in Fig. 2. The enstrophy growth in the early stage is not monotonic, showing instead a few local maxima. Its largest peak is reached at around $t \approx 4$. This is just preceded by the deepest minimum in $f_{\min}$, which attains negative values throughout the simulation. The enstrophy $Q(t)$ gradually declines due to viscous effects after this fluctuating period, which ends at $t \approx 10$, while $f_{\min}$ steadily tends to zero as viscous effects become dominant over non-linear ones.

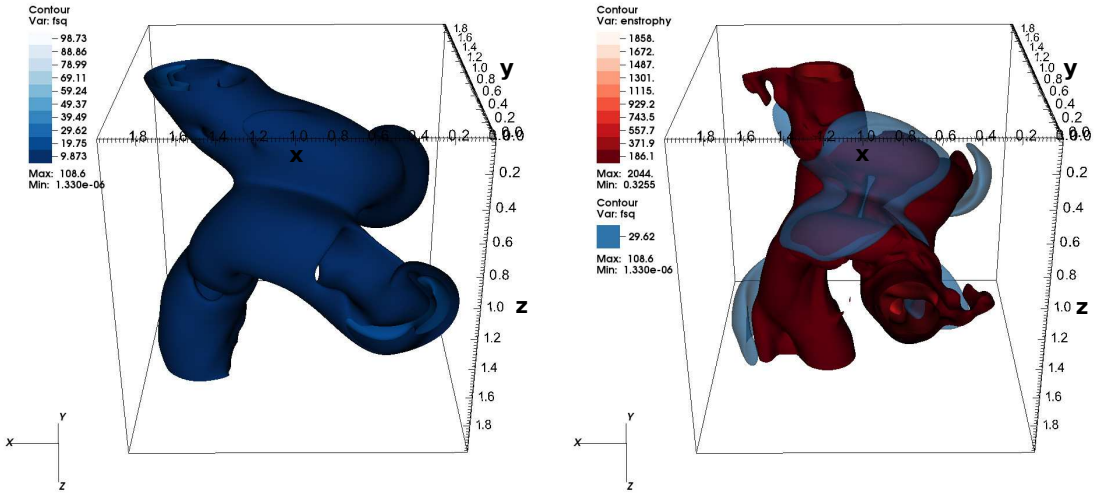

(a) (b)

Figure 3. Isosurfaces of (a) $|\boldsymbol{f}|^2$ (blue) and (b) $|\boldsymbol{f}|^2$ (blue, with transparency) overlaid on $|\boldsymbol{\omega}|^2$ (red) at $t = 5.0$. In (b) the $|\boldsymbol{f}|^2$ overlaid isosurface is in the mid-range.

As seen in Figure 3, the isosurfaces of (a) $|\boldsymbol{f}|^2$ at a later time $t = 5.0$ still resemble, to some degree, those observed in the enstrophy, with the two vortex tubes interacting. The correlation between the two quantities is more obvious in (b), showing the isosurface of $|\boldsymbol{f}|^2$ at a specifically selected threshold, overlaid on the enstrophy at the same time $t = 5.0$. The bridging phenomenon observed in $|\boldsymbol{\omega}|^2$, which is well developed at this stage, is known as a precursor for eventual vortex reconnection, see e.g. [8]. The chosen $|\boldsymbol{f}|^2$ isosurface encompasses the bridging regions and the interacting zone between the tubes, as well as wrapping around the tubes themselves.

Similarly, Fig. 4 shows the isosurfaces for (a) $|\boldsymbol{T}[\nabla\psi]|^2$ and (b) those for $|\boldsymbol{T}[\nabla\psi]|^2$ at a specifically selected threshold, overlaid on the enstrophy at the same time $t = 5.0$. The isosurfaces of $|\boldsymbol{T}[\nabla\psi]|^2$ are seen to exhibit a dipole structure around the vortex tubes, each one of dipole's branches closely corresponding to the vortex tubes. However, the overlay with the enstrophy shows that large values of $\boldsymbol{T}[\nabla\psi]$ are mostly located in the dipole branches that do not correspond to the enstrophy vortex tubes, and the distribution of $\boldsymbol{T}[\nabla\psi]$ appears more broadly scattered compared to that of the potential term $\boldsymbol{f}$.

These observations are consistent with what has been reported in the case of two-dimensional Navier-Stokes equations [1]. There the corresponding potential term $\boldsymbol{f}$

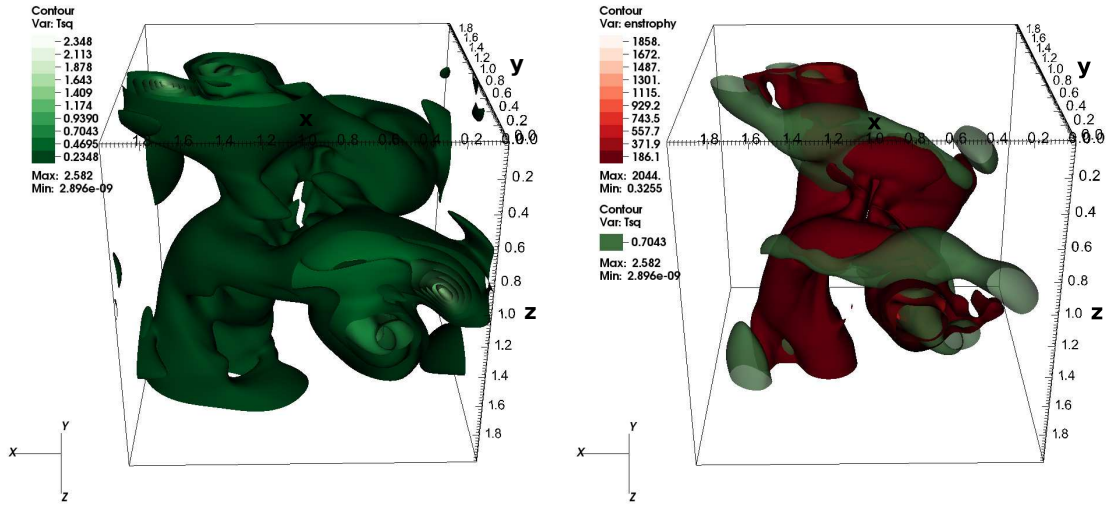

(a) (b)

Figure 4. Isosurfaces of (a) $|\boldsymbol{T}|^2$ (green) and (b) $|\boldsymbol{T}|^2$ (green, with transparency) overlaid on $|\boldsymbol{\omega}|^2$ (red) at $t = 5.0$. In (b) the $|\boldsymbol{T}|^2$ overlaid isosurface is in the mid-range.

shows a strong correlation with thin filaments possessing large vorticity gradients, whereas the distribution of the nonlinear term $\boldsymbol{T}[\nabla\boldsymbol{\psi}]$ is less concentrated but scattered outside of the coherent vortices.

4.3. Case 2: Decaying isotropic turbulence

Next we present results for the case of a random initial condition leading to decaying isotropic turbulence. Figure 5 presents the time evolution of $Q(t)$ and $f_{\min}$; the enstrophy is seen to increase monotonically before reaching a maximum at around $t \approx 3$, which is followed by a gradual decline. The peak in $Q(t)$ is once again preceded by the deepest minimum in $\boldsymbol{f}$, which occurs at $t \approx 2$.

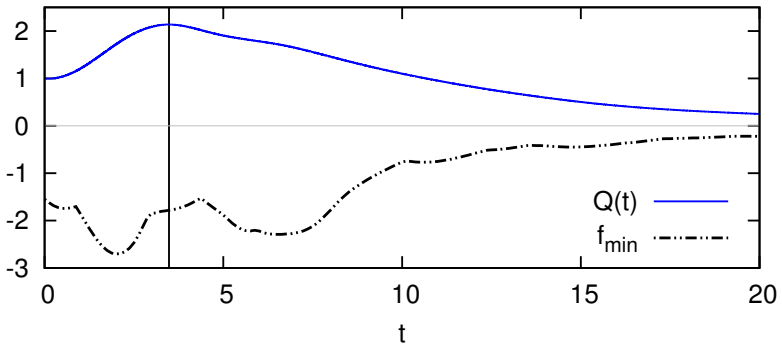

Figure 5. Time evolution of $Q(t)$ (blue, full line) and $f_{\min}$ (black, dot-dashed) for isotropic turbulent initial conditions.

In the early stages, the flow field consists of vorticity layers as seen in Fig 6, showing the isosurfaces of (a) enstrophy $|\boldsymbol{\omega}|^2$ and $|\boldsymbol{f}|^2$ and (b) enstrophy $|\boldsymbol{\omega}|^2$ and $|\boldsymbol{T}[\nabla\boldsymbol{\psi}]|^2$

at time $t = 1.25$. The isosurfaces of $|\boldsymbol{f}|^2$ show a close correlation to those of the intense enstrophy in (a), whereas those of $|\boldsymbol{T}[\nabla\psi]|^2$ are more broadly scattered between vorticity layers in (b). Those features are similar to the results from Case 1.

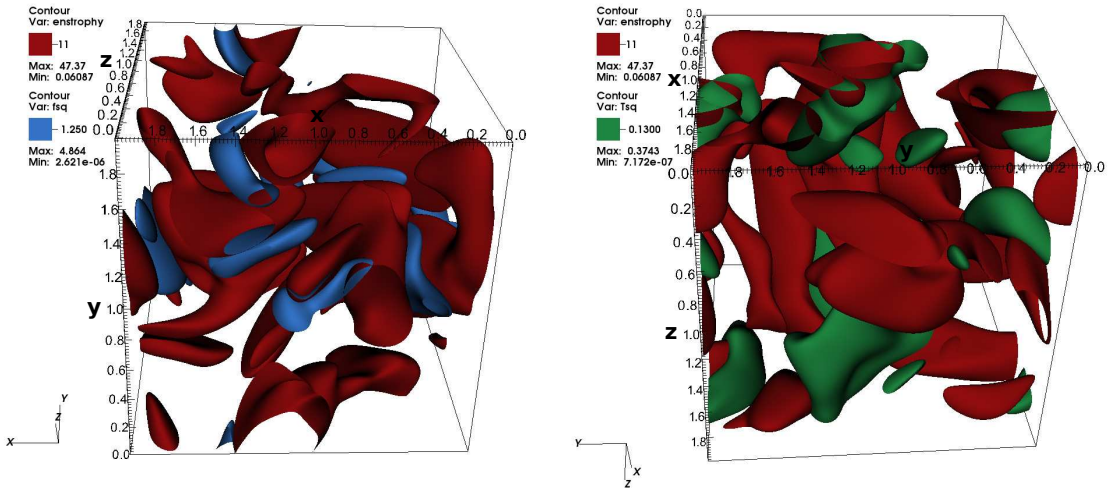

(a) (b)

Figure 6. Isosurfaces of (a) $|\boldsymbol{\omega}|^2$ (red) and $|\boldsymbol{f}|^2$ (blue) and (b) $|\boldsymbol{\omega}|^2$ (red) and $|\boldsymbol{T}|^2$ (green) for $t = 1.25$. The isosurface used for $|\boldsymbol{\omega}|^2$ is the same, but different angles are used to better reveal the correlations with $|\boldsymbol{f}|^2$ and $|\boldsymbol{T}|^2$.

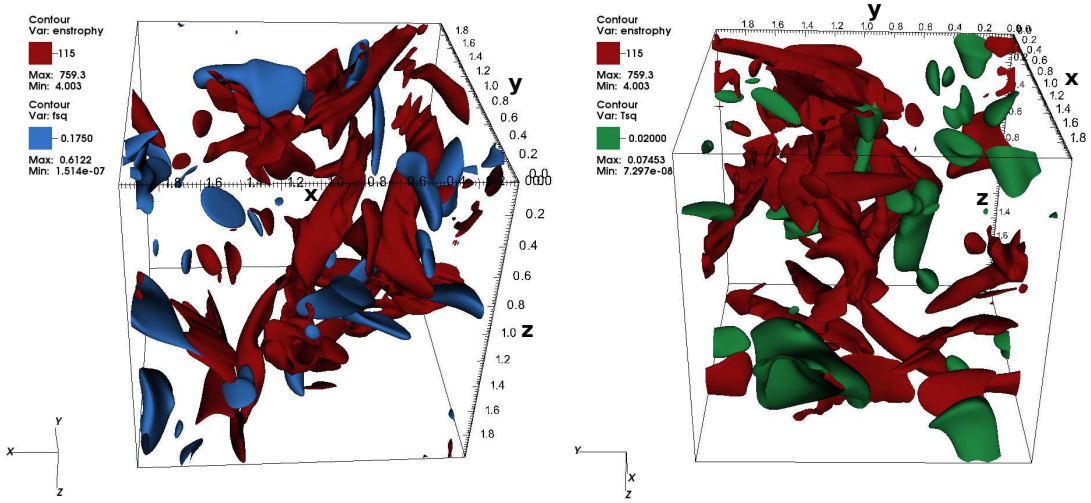

(a) (b)

Figure 7. Isosurfaces of (a) $|\boldsymbol{\omega}|^2$ (red) and $|\boldsymbol{f}|^2$ (blue) and (b) $|\boldsymbol{\omega}|^2$ (red) and $|\boldsymbol{T}|^2$ (green) for $t = 10.0$. The isosurface used for $|\boldsymbol{\omega}|^2$ is the same, but different angles are used to better reveal the correlations with $|\boldsymbol{f}|^2$ and $|\boldsymbol{T}|^2$.

In the late stage of decaying isotropic turbulence, it is generally understood that the flow consists of vorticity tubes rather than vorticity layers. In Fig. 7, which shows isosurfaces for the same quantities as in Fig. 6 but for a later time $t = 10.0$, the

isosurfaces of the enstrophy indeed appear to be tube-like rather than layer-like. In this instance, some of the isosurfaces of the potential term $|\boldsymbol{f}|^2$ appear in the vicinity of high enstrophy regions, but not all, meaning that the correlation between the two quantities is weaker than in Fig. 6. A substantial decay has taken place by $t = 10$, where $Q(t)$ has decreased by a factor of two and $f_{\min}(t)$ by a factor of three. This explains why a weaker correlation between $|\boldsymbol{\omega}|^2$ and $|\boldsymbol{f}|^2$ is observed. The $|\boldsymbol{T}|^2$ isosurfaces, on the other hand, remain scattered around regions with intense vorticity.

5. Summary

By recasting the Navier-Stokes equations as the heat equations with the potential term $\boldsymbol{f}$, we have studied the role played by the potential term in the characterisation of the flow fields. In view of the fact that the potential term controls regularity properties of solutions, it is expected that the $\boldsymbol{f}$ term can monitor near-singular behaviour in turbulent flows. We have hence studied how the potential term behaves by direct numerical simulations. It is found that the components of $\boldsymbol{f}$ tend to take negative values, reducing the value of $\boldsymbol{\theta}$, and thus making $\psi_j = k \log \theta_j$ potentially near-singular. In this paper such an expectation has been demonstrated in the sense that they do detect regions of intensely interacting vorticity and their proximity.

In one experiment where the orthogonal vortex tubes initial condition is used, we found that the bridging phenomenon in a process of vortex reconnection is well captured by the large (negative) value of $\boldsymbol{f}$, and a strong correlation is observed between $\boldsymbol{f}$ and the enstrophy, while the non-linear term $\boldsymbol{T}[\nabla\boldsymbol{\psi}]$ appeared more scattered around the vorticity. A temporal analysis also revealed that the largest (most negative) value of $\boldsymbol{f}$ shortly precedes the maximum in the enstrophy $Q(t)$, again indicating that they are strongly correlated.

The other experiment used random initial conditions leading to decaying turbulence; in this case, during the early developing stages, regions possessing large $|\boldsymbol{f}|$ values are strongly correlated with vorticity layers. Later, after the turbulence has well-developed, such a correlation between $\boldsymbol{f}$ and vorticity – which now predominantly features vortex tubes, rather than sheets – has weakened due to the diminishing importance of the nonlinear term against the viscous dissipative term. The behaviour of the potential term $\boldsymbol{f}$ is different from that of the nonlinear term $\boldsymbol{T}[\nabla\boldsymbol{\psi}]$, whose correlation with the enstrophy is instead found to be weaker in both conditions at all times, its values being scattered around the enstrophy. Once again, the temporal evolution of $\boldsymbol{f}$ and $Q(t)$ showed the largest (most negative) value of the former being closely followed by the maximum enstrophy value, before this declined gradually.

It is of interest to study whether this method can be used as identification of extreme events in turbulence at much higher Reynolds numbers.

Acknowledgement

This work has been supported by an EPSRC grant EP/N022548/1, including a research associate position for Riccardo Vanon.

References

[1] K. Ohkitani, *Analogue of the Cole-Hopf transform for the incompressible Navier-Stokes equations and its application*, Journal of Turbulence, 18 (2017), 465–479.

[2] J.D. Cole, *On a linear quasilinear parabolic equation in aerodynamics*, Q. Appl. Math. 9 (1951), pp. 225–236.

[3] E. Hopf, *The partial differential equation* $u_t + uu_x = \mu u_{xx}$, Commun. Pure Appl. Math. 3 (1950), pp. 201–230.

[4] K. Ohkitani, *Dynamical equations for the vector potential and the velocity potential in incompressible irrottational Euler flows: a refined Bernoulli theorem*, Phys. Rev. E. 92 (2015), 033010.

[5] K. Ohkitani, *Characterization of blowup for the Navier-Stokes equations using vector potentials*, AIP Advances, 7 (2017), 015211.

[6] K. Ohkitani, *Cole-Hopf–Feynman-Kac formula and quasi-invariance for Navier-Stokes equations*, J. Phys. A: Math. Theor., 50 (2017) 405501.

[7] O.N. Boratav, R.B. Pelz and N.J. and N. Zabusky, *Reconnection in orthogonally interacting vortex tubes: Direct numerical simulations and quantifications,* Phys. Fluids A, 4 (1992) 581–605.

[8] S. Kida and M. Takaoka, *Vortex reconnection,* Ann. Rev. Fluid Mech., 26 (1994) 169–177.

[9] R.E. Caflisch, I. Klapper and G. Steele, *Remarks on singularities, dimension and energy dissipation for ideal hydrodynamics and MHD,* Commun. Math. Phys., 184 (1997) 443–455.

Appendix A. MHD equations written in vector and magnetic potentials

In standard notations, the MHD equations take the following form:

$$\frac{\partial \boldsymbol{u}}{\partial t} + \boldsymbol{u}\cdot\nabla\boldsymbol{u} = -\nabla p + \boldsymbol{J}\times\boldsymbol{B} + \nu\triangle\boldsymbol{u}, \tag{A1}$$

$$\frac{\partial \boldsymbol{B}}{\partial t} + \boldsymbol{u}\cdot\nabla\boldsymbol{B} = \boldsymbol{B}\cdot\nabla\boldsymbol{u} + \eta\triangle\boldsymbol{B}, \tag{A2}$$

$$\nabla\cdot\boldsymbol{u} = \nabla\cdot\boldsymbol{B} = 0,$$

$$\boldsymbol{u}(\boldsymbol{x},0) = \boldsymbol{u}_0(\boldsymbol{x}), \quad \boldsymbol{B}(\boldsymbol{x},0) = \boldsymbol{B}_0(\boldsymbol{x}),$$

where $\boldsymbol{J} = \nabla\times\boldsymbol{B}$. Equation (A1) can be rewritten as

$$\frac{\partial \boldsymbol{u}}{\partial t} = \boldsymbol{u}\times\boldsymbol{\omega} + \boldsymbol{J}\times\boldsymbol{B} - \nabla\left(p + \frac{|\boldsymbol{u}|^2}{2}\right) + \nu\triangle\boldsymbol{u},$$

by $\nabla\frac{|\boldsymbol{u}|^2}{2} = \boldsymbol{u}\cdot\nabla\boldsymbol{u} + \boldsymbol{u}\times\boldsymbol{\omega}$, and it follows that

$$\frac{\partial \boldsymbol{\omega}}{\partial t} = \nabla\times(\boldsymbol{u}\times\boldsymbol{\omega}) + \nabla\times(\boldsymbol{J}\times\boldsymbol{B}) + \nu\triangle\boldsymbol{\omega}.$$

By inverting the Laplacian operator and using the relation $\boldsymbol{\psi} = -\triangle^{-1}\boldsymbol{\omega}$, we have

$$\frac{\partial \boldsymbol{\psi}}{\partial t} = -\triangle^{-1}\nabla\times(\boldsymbol{u}\times\boldsymbol{\omega}) - \triangle^{-1}\nabla\times(\boldsymbol{J}\times\boldsymbol{B}) + \nu\triangle\boldsymbol{\psi},$$

or

$$\frac{\partial \boldsymbol{\psi}}{\partial t} = \boldsymbol{T}[\nabla \boldsymbol{\psi}] - \boldsymbol{T}[\nabla \boldsymbol{A}] + \nu \triangle \boldsymbol{\psi}, \tag{A3}$$

where $\boldsymbol{u} = \nabla \times \boldsymbol{\psi}$ and $\boldsymbol{B} = \nabla \times \boldsymbol{A}$. The definition of $\boldsymbol{T}[\nabla \boldsymbol{\psi}]$ remains the same as for the Navier-Stokes equations.

On the other hand, (A2) is equivalent to

$$\frac{\partial \boldsymbol{B}}{\partial t} = \nabla \times (\boldsymbol{u} \times \boldsymbol{B}) + \eta \triangle \boldsymbol{B},$$

from which it follows that

$$\frac{\partial \boldsymbol{J}}{\partial t} = -\triangle (\boldsymbol{u} \times \boldsymbol{B}) + \nabla \left(\nabla \cdot (\boldsymbol{u} \times \boldsymbol{B}) \right) + \eta \triangle \boldsymbol{J}.$$

Again, by inverting the Laplacian, we find

$$\frac{\partial \boldsymbol{A}}{\partial t} = \boldsymbol{u} \times \boldsymbol{B} - \triangle^{-1} \nabla \left(\nabla \cdot (\boldsymbol{u} \times \boldsymbol{B}) \right) + \eta \triangle \boldsymbol{A},$$

that is,

$$\frac{\partial \boldsymbol{A}}{\partial t} = (\nabla \times \boldsymbol{\psi}) \times (\nabla \times \boldsymbol{A}) + \boldsymbol{S}[\nabla \boldsymbol{\psi}, \nabla \boldsymbol{A}] + \eta \triangle \boldsymbol{A}, \tag{A4}$$

where $\boldsymbol{\omega} = -\triangle \boldsymbol{\psi}$ and $\boldsymbol{J} = -\triangle \boldsymbol{A}$. The integral operator $\boldsymbol{S}[\nabla \boldsymbol{\psi}, \nabla \boldsymbol{A}]$ is defined by

$$\boldsymbol{S}[\nabla \boldsymbol{\psi}, \nabla \boldsymbol{A}] = (-\triangle)^{-1} \nabla (\nabla \cdot \boldsymbol{w}),$$

where $\boldsymbol{w} = \boldsymbol{u} \times \boldsymbol{B}$. For its explicit representation, we recall the following dipole-potential formula, where ϕ is a solution of $\triangle \phi(\boldsymbol{x}) = f(\boldsymbol{x})$. It reads

$$\frac{\partial^2 \phi}{\partial x_i \partial x_j} = \frac{f(\boldsymbol{x})}{3} \delta_{ij} + \frac{1}{4\pi} \mathrm{P.V.} \int \left(\frac{\delta_{ij}}{|\boldsymbol{x} - \boldsymbol{y}|^3} - \frac{3(x_i - y_i)(x_j - y_j)}{|\boldsymbol{x} - \boldsymbol{y}|^5} \right) f(\boldsymbol{y}) \mathrm{d}\boldsymbol{y},$$

which is obtained by taking the second-order derivatives of the Newtonian potential. Taking $\boldsymbol{f} = -\boldsymbol{w}$, we find

$$S_i = -w_i(\boldsymbol{x}) - \frac{1}{4\pi} \mathrm{P.V.} \int \left(\frac{w_i(\boldsymbol{y})}{|\boldsymbol{x} - \boldsymbol{y}|^3} - \frac{3(x_i - y_i)(x_j - y_j) w_i(\boldsymbol{y})}{|\boldsymbol{x} - \boldsymbol{y}|^5} \right) \mathrm{d}\boldsymbol{y}.$$

Finally, we note that in terms of $\nabla \boldsymbol{\psi}$ and $\nabla \boldsymbol{A}$, we can write

$$w_i = \epsilon_{ijk} (\epsilon_{jlm} \partial_l \psi_m)(\epsilon_{kpq} \partial_p A_q) = \frac{1}{2} \epsilon_{kpq} (\partial_k \psi_i - \partial_i \psi_k)(\partial_p A_q - \partial_q A_p).$$

Appendix B. Cole-Hopf transform for MHD equations

We consider Cole-Hopf transforms $\psi_j = k \log \theta_j$ and $A_j = l \log \chi_j$ $(j = 1, 2, 3)$, where k and l are constants. Equation (A3) is equivalent to

$$\frac{\partial \theta_j}{\partial t} = \nu \triangle \theta_j + f_j \left[\frac{\nabla \theta}{\theta}, \frac{\nabla \chi}{\chi} \right] \theta_j, \quad \text{(no summation)} \tag{B1}$$

where we have defined

$$f_j \left[\frac{\nabla \theta}{\theta}, \frac{\nabla \chi}{\chi} \right] \equiv k T_j \left[\frac{\nabla \theta}{\theta} \right] - \nu \frac{|\nabla \theta_j|^2}{\theta_j^2} + \frac{l^2}{k^2} T_j \left[\frac{\nabla \chi}{\chi} \right], \quad (j = 1, 2, 3). \tag{B2}$$

Here, for simplicity, we have introduced the following abbreviations:

$$\frac{\nabla \theta}{\theta} \equiv \left\{ \frac{\nabla \theta_1}{\theta_1}, \frac{\nabla \theta_2}{\theta_2}, \frac{\nabla \theta_3}{\theta_3} \right\}, \quad \frac{\nabla \chi}{\chi} \equiv \left\{ \frac{\nabla \chi_1}{\chi_1}, \frac{\nabla \chi_2}{\chi_2}, \frac{\nabla \chi_3}{\chi_3} \right\}.$$

Furthermore, (A4) can be rewritten as

$$\frac{\partial \chi_j}{\partial t} = \eta \triangle \chi_j + g_j \left[\frac{\nabla \theta}{\theta}, \frac{\nabla \chi}{\chi} \right] \chi_j, \quad \text{(no summation)}, \tag{B3}$$

where

$$g_j \left[\frac{\nabla \theta}{\theta}, \frac{\nabla \chi}{\chi} \right] = k S_j \left[\frac{\nabla \theta}{\theta}, \frac{\nabla \chi}{\chi} \right] + k \left(\nabla \times \log \theta \right) \times \left(\nabla \times \log \chi \right)|_j - \eta \frac{|\nabla \chi_j|^2}{\chi_j^2}, \quad (j = 1, 2, 3), \tag{B4}$$

with the following abbreviation

$$\left(\nabla \times \log \theta \right) \times \left(\nabla \times \log \chi \right)|_j \equiv \epsilon_{jkl} (\epsilon_{kpq} \partial_p \log \theta_q)(\epsilon_{lmn} \partial_m \log \theta_n).$$

It is straightforward to derive regularity criteria for solutions of the MHD equations; if the following conditions

$$\int_0^T \sup_{\boldsymbol{x}} |\boldsymbol{f}(\boldsymbol{x}, t)| dt < \infty \ \text{ and } \ \int_0^T \sup_{\boldsymbol{x}} |\boldsymbol{g}(\boldsymbol{x}, t)| dt < \infty$$

are satisfied, then the solutions are regular on $[0, T]$. In fact, under the conditions of boundedness for $\boldsymbol{f}$ and $\boldsymbol{g}$, they serve as martingales and the conclusion follows by applying the Feynman-Kac formulas to (B1, B3). Note that, in standard variables, the above conditions correspond roughly to

$$\text{“} \int_0^T (\|\boldsymbol{u}\|_\infty^2 + \|\boldsymbol{B}\|_\infty^2) dt < \infty \text{”} \ \text{ and } \ \text{“} \int_0^T \|\boldsymbol{u}\|_\infty \|\boldsymbol{B}\|_\infty dt < \infty \text{”},$$

respectively. It may be of interest to derive these more directly from the MHD equations. See, e.g. [9].